Int. J. Electrochem. Sci., 13 **(2018)** 3107 – 3123, doi: 10.20964/2018.03.16

International Journal of
ELECTROCHEMICAL
SCIENCE
www.electrochemsci.org

Effect of Surface Roughness on Pitting Corrosion of 2A12 Aluminum Alloy

Wenming Tian[*], *Bingxuan Chao, Xiyao Xiong, Zhiyong Li*

AVIC Changhe Aircraft Industry (Group) Corporation LTD, No. 539 Zhushan Road, Jingdezhen, Jiangxi 333002, P. R. China
[*]E-mail: tianwenming.dhr@163.com

Received: 21 November 2017 / *Accepted:* 6 January 2018 / *Published:* 5 February 2018

The microstructure and pitting corrosion of 2A12 aluminum alloy abraded in one-direction with abrasive paper of various grit numbers were investigated. Statistical analysis indicated that abrasion can alter surface roughness and induce partial dissolution of intermetallic particles. The electrochemical inhomogeneity resulted from intermetallic particles and roughness had significantly impact on pitting corrosion of 2A12 aluminum alloy. All the samples underwent pitting corrosion, while surface layer dissolution (except pitting) was not observed. The enhanced density, higher area friction and bigger size of Al_2CuMg particles (S-phase) on the rougher surface made it more susceptible to pitting.

Keywords: A. Aluminum; B. Intermetallic particles; C. Roughness; D. Pitting corrosion. E. Electrochemical measurement

1. INTRODUCTION

2A12 aluminum alloy is a kind of Al-Cu-Mg alloy, and widely used in aircraft industry, because of its low density and high specific strength [1-5]. Due to the reactive nature of aluminum and magnesium, the corrosion resistance of 2A12 alloy has attracted much attention [6-9]. Generally, 2A12 aluminum alloy exhibited good corrosion resistance to general corrosion, which is attributed to the oxide film. However, it is liable to undergo localized corrosion such as pitting, intergranular corrosion and exfoliation corrosion [7-9]. Ascribed to the difficulty in detection and prediction, a small narrow pit could result in failure of an entire engineering system. Potentiodynamic and potentiostatic polarization are powerful techniques for investigation of pitting. Pitting potential (E_{pit}) and sometimes breakdown potential obtained by potentiodynamic polarization are most commonly used to evaluate pitting susceptibility, whereas E_{pit} fails to quantify the number and size of pits (stable and metastable)

[10-14]. Potentiostatic polarization can provide quantitative and mechanistic information by measureable current transients associated with pit initiation, propagation and repassivation [10-15].

The initial stages of corrosion are strongly associated with surface conditions [14-18]. During many industrial processes such as rolling, machining and grinding, the surface undergoes severe plastic deformation (SPD), which resulted in formation of deformed surface layer (DSL). The microstructure and microchemistry of DSL on aluminium alloys are often different from those of bulk matrix in terms of grain size, intermetallic particle distribution and oxide inclusions [16-26]. For example, hot and cold rolling could induce a significant microstructure refinement in DSL [18-21]. Thompson [18] and Nisancioglu [19] revealed that SPD in rolled surface layer promoted fine dispersion of intermetallics during subsequent heat treatment. Formation of nano-sized sub-grains with the redistribution of alloying elements was observed in the DSL with thickness of several hundred nanometers [16, 17, 25, 26]. The redistribution of alloying elements was resulted in dissolution and crush of precipitates during abrasion [16, 17, 25, 26].

It is generally accepted that the corrosion behavior of aluminum alloys is closely related to the electrochemical inhomogeneity resulted from intermetallic precipitates and roughness [5-8, 12, 27-31]. For instance, Hughes [30] revealed that the electrochemical activity difference between the matrix and S-phase could induce the formation of a stable pit. Grilli [29] reported that the pitting attack concentrated at the Al matrix adjacent to Al-Cu-Mn-Fe particles, and revealed that S-phase acted as pitting initiation sites in 2219 alloy. By altering the microstructure and microchemistry of DSL, SPD shows strong impact on corrosion behavior of aluminium alloys. The enhanced density of intermetallic particles in the surface layer generated during rolling made the rolled aluminium alloys susceptible to superficial corrosion [19-21]. Potentiodynamic polarization tests of a rolled Al-Fe-Si-Mn alloy revealed that both the anodic and cathodic reactivity of the deformed surface layer of a rolled aluminum alloy were significantly higher than those of the bulk alloy [21]. By in situ observation during polarization of AA7075 aluminum alloys, Frankel [26] found that two breakdown potentials were associated with dissolution of active surface layer and localized corrosion. With grit number increasing, potentiodynamic polarization tests revealed the DSL became less susceptible to pitting [16]. Furthermore, due to the higher Cu content, the DSL on overaged 2A12 alloy exhibited slightly decreased the pitting susceptibility compared to the underlying matrix [17].However, the roughness and DSL caused by surface abrasion on 2A12 aluminum alloy and corresponding corrosion behavior have barely been reported. Additionally, to our best knowledge, there are few literatures focus on statistical analyses of intermetallic precipitates and the quantitative investigation of pits (number and size of stable and metastable pits) in aluminium alloys with different surface roughness created by abrasion.

In this study, the samples of 2A12 aluminum alloy were manually abraded with abrasive paper of various grit numbers to obtain different surface roughness. The effect of surface abrasion on the pitting corrosion of 2A12 aluminum alloy was evaluated by electrochemical methods including potentiodynamic polarization, electrochemical impedance spectroscopy (EIS) measurements and potentiostatic polarization. The intermetallic particles in DSL, current transients (metastable pitting) and stables pits were statistically analyzed.

2. EXPERIMENTAL

2.1 Sample preparation

2A12 aluminum alloy rolled plate with thickness of 60 mm was used in this work. The samples were obtained by cutting from an area near one- sixth in reference to the plate thickness. The abrasion of the samples was carried out in one-direction using stationary silicon carbide papers with girt number of 600, 2000 and 5000. To minimize corrosion, ethyl alcohol was used during surface abrasion. The samples were then cleaned ultrasonically in acetone and ethyl alcohol, respectively and dried by warm flowing air.

2.2 Microstructure measurements

The surface roughness of sanded samples was examined perpendicular to the abrasion direction with a scan length of 5mm using surface texture measuring instrument (Marsurf M300C, Germany). The microstructure of sanded samples was studied by field-emission scanning electron microscope (SEM; JEOL 7500, Japan) equipped with energy dispersive X-ray spectroscopy (EDS; INCA PentaFETx3, Britain). The size and number of intermetallic precipitates from low magnification images and high magnification images were statistically analyzed using ImageJ software.

2.3 Electrochemical tests

The electrochemical tests were performed on an electrochemical workstation (AUTALAB PGSTAT 302N) using a classical three-electrode configuration, which comprises a platinum sheet as the counter electrode, a saturated calomel electrode (SCE) as the reference electrode and the sanded samples as the working electrode. All of the electrochemical tests were carried out in borate-buffered solution (pH=7.2) containing 0.0001M NaCl.

The samples with surface area of 1 cm^2 were employed for potentiodynamic polarization and EIS measurements. Potentiodynamic polarization measurements were performed by changing the electrode potential from 200 mV below the open circuit potential (OCP) into positive direction at a scan rate of 1$mV \cdot s^{-1}$ until the anodic current density reached 0.1 $mA \cdot cm^{-2}$. Tafel extrapolation was employed to analyze the polarization data. The EIS measurements were carried out using a 10 mV AC stimulus signal in the frequency range from 100 kHz to 10 mHz. The EIS spectra were fitted by using ZSimpWin software.

In consideration of the background noise current and surface grooves, 1 mm diameter samples were used in potentiostatic polarization for current transient measurements. The current signal was recorded at a frequency of 1000 Hz with 1000 s polarization duration at 100 mV below the E_{pit}. In order to estimate the stable pits, the sanded samples with exposed surface area of 1 cm^2 were polarized at the E_{pit} with 3600 s polarization duration. The morphologies of stable pits were examined by SEM and optical microscope. Statistical analysis of the pits size was performed using optical

microphotographs. In order to ensure reproducibility, the measurements were performed at least in triplicate.

3. RESULTS

3.1 Surface roughness

The surface morphologies of 2A12 aluminum alloy abraded with abrasive paper of 600 grit, 2000 grit and 5000 grit in one-direction are presented in Fig. 1.

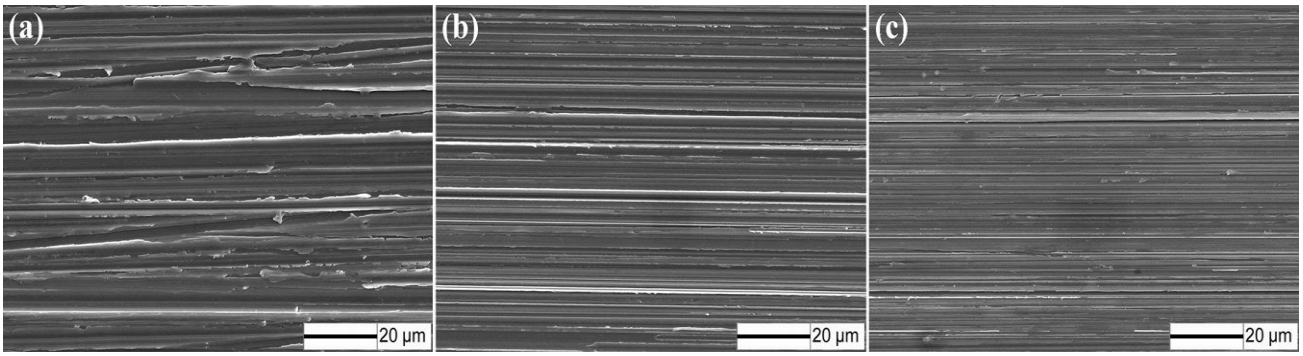

Figure 1. Secondary electron SEM images of 2A12 aluminum alloy abraded with abrasive papers of (a) 600 grit, (b) 2000 grit and (c) 5000 grit.

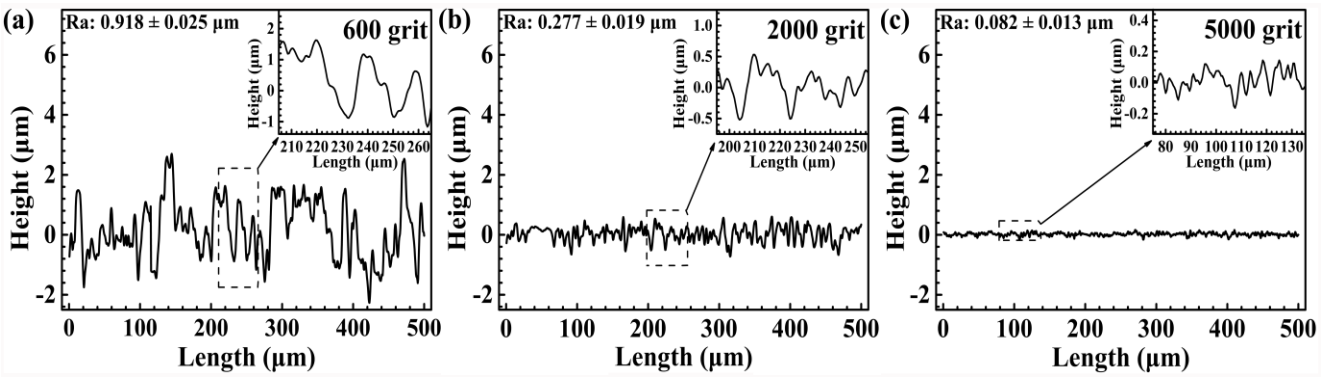

Figure 2. The surface profiles of 2A12 aluminum alloy abraded with abrasive papers of (a) 600 grit, (b) 2000 grit and (c) 5000 grit.

Regularly oriented grooves and elongated ridges were observed on the surface of the sanded samples. Their appearance was attributed to removal of material, which was evidence of SPD. The surface roughness measurements were carried out perpendicular to the abrasion direction, from which the surface profiles were obtained, as shown in Fig. 2. With increasing grit number from 600 to 5000, ascribed to the decrease in the average particle size of abrasive papers, the depth and width of the grooves decreased. This meant that the increase of grit number resulted in a smoother surface, i.e. whereas the decrease of girt number would result in a rougher surface. The average roughness

parameter (*R*a) of samples abraded with abrasive papers of 600 grit, 2000 grit and 5000 grit were 0.918 μm, 0.277 μm and 0.082 μm, respectively. As expected, there was a trend that *R*a decreased with increasing grit number from 600 to 5000.

3.2 Microstructure of sanded samples

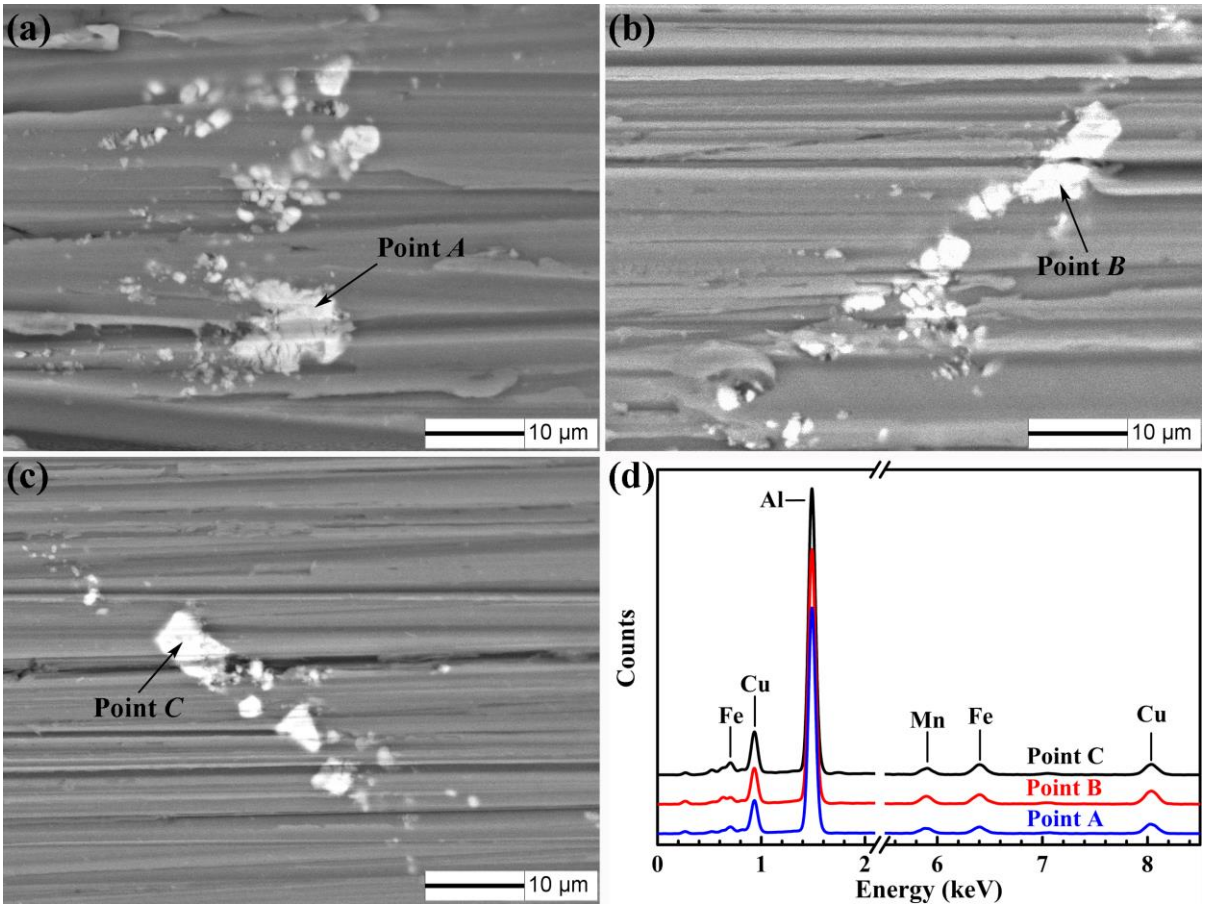

Figure 3. Backscattered electron SEM images of 2A12 aluminum alloy abraded with abrasive papers of (a) 600 grit, (b) 2000 grit and (c) 5000 grit; (d)EDS results of point *A*, point *B* and point *C* .

The backscattered electron SEM images of 2A12 aluminum alloy abraded with abrasive paper of different grit numbers are presented in Fig. 3. The white contrast speckles implied the presence of intermetallic particles which were rich in heavy elements. The EDS spectra (Fig. 3d) showed high intensity of Al, Cu, Mg, indicating that the intermetallic particles are S-phase. The average composition of the intermetallic particles was 60% Al, 18% Cu, 22% Mg (by atoms).

Considering the size of intermetallic particles, 30 low magnification (×200) images and 10 high magnification (×5000) images were used to statistically analyze the size and density of intermetallic particles for each kind of sanded samples. The size distribution of intermetallic particles is shown in Fig. 4. Detail statistical data of intermetallic particles are listed in Table 1. The average particle size in 2A12 aluminum alloy abraded with abrasive papers of 600 grit, 2000 grit and 5000 grit were 778 nm, 636 nm and 554 nm, respectively. Similarly, the area fraction of intermetallic particles in 2A12

aluminum alloy abraded with abrasive papers of 600 grit, 2000 grit and 5000 grit were 0.386%, 0.245% and 0.119%, respectively. The average size of intermetallic particles decreased with increasing grit number from 600 to 5000. Besides, the area fraction and population density of intermetallic particles had the same trend as the average particle size.

Table 1. Statistical data of intermetallic particles in 2A12 aluminum alloy abraded with abrasive paper of various grit numbers.

Grit number	Density (count·μm^{-2})	Area fraction (%)	Average particle size (μm)
600	0.00136	0.386	0.778
2000	0.00096	0.245	0.636
5000	0.00064	0.119	0.554

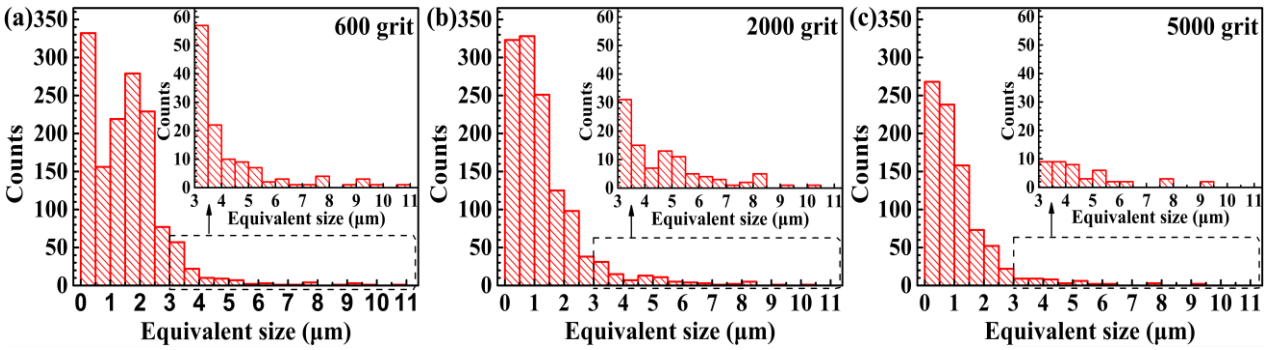

Figure 4. Intermetallic particle size distribution histograms in 2A12 aluminum alloy abraded with abrasive papers of (a) 600 grit, (b) 2000 grit and (c) 5000 grit.

The change in density and average size of intermetallic particles might be attributed to the dissolution and crush of intermetallic particles associated with dislocation motion induced by SPD. Accompanied by temperature rise, the shear strain destroyed fine particles and damaged large ones. Consequently, large intermetallic particles might break into smaller particles and small particles might be partially eliminated. In fact, the strain-induced dissolution of precipitates involved two processes: the dissolution and reformation of precipitates [32-35]. The dislocation shearing event dissolved the precipitates and drove the solute atoms into solution. If there was sufficient time before the next shearing dislocation arrives, the solute atoms could diffuse back to the precipitate, which resulted in recovery of precipitates. With increase of grit number, the removal of material and the intervals between dislocation shearing events decreased, i.e. the smoother surface layer underwent more dislocation shearing events with shorter intervals. The dislocation segregated the solute atoms which retarded the reformation of precipitates. Accordingly, with increasing grit number from 600 to 5000, more intermetallic particles were dissolved. Therefore, compared to the smoother surface, the rougher surface contained more S-phase with relatively bigger size. Similar phenomena were observed in surface layer of aluminium alloys during rolling and abrasion [32-35].

3.3 Potentiodynamic polarization tests

The potentiodynamic polarization curves of the sanded samples after 30 min immersion in borate-buffered 0.0001 M NaCl solution are presented in Fig. 5. The polarization curves had a similar shape, which indicated that all the samples went through the same corrosion reactions. One obvious breakdown potential, E_{pit}, exhibited in all the curves of samples abraded with abrasive papers of 600 grit, 200grit and 5000grit. The E_{pit} was found to be much higher than the corrosion potential (E_{corr}), which indicated that all of the sanded samples exhibited passivation behavior and showed clear passive ranges. With increasing grit number from 600 to 5000, a shift in E_{corr} and E_{pit} to more noble values was detected, while the shift in E_{pit} (about 200mV) was relatively larger than that in E_{corr} (about 86 mV). Therefore, with increasing grit number from 600 to 5000, the passive ranges of 2A12 aluminum alloy increased.

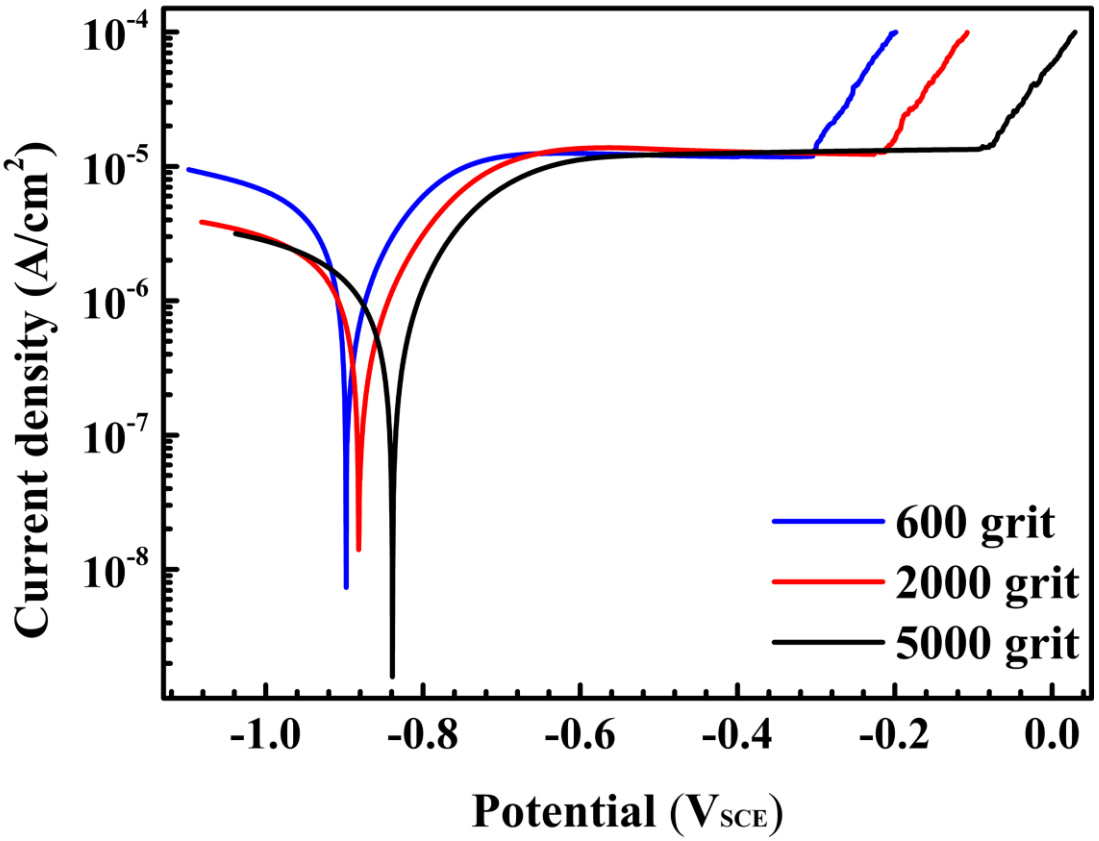

Figure 5. Potentiodynamic polarization curves of 2A12 aluminum alloy abraded with abrasive paper of various grit numbers.

Within the over-potential range from tens to a hundred millivolts relative to the E_{corr}, the log current density increased linearly with applied over-potential i.e., Tafel-type behavior. Therefore, Tafel extrapolation was employed to analyze the polarization curves. The relevant results are summarized in Table 2. With increasing grit number from 600 to 5000, the E_{corr} increased about 86 mV, and the corrosion current density (i_{corr}) decreased, implying a smaller corrosion susceptibility of the smoother surface. The mean values of anodic Tafel slope (b_a) were between 143 mV·dec^{-1} and 161 mV·dec^{-1},

which were much higher than the value of 20-30 mV·dec^{-1} caused by Al oxidation to Al^{3+}, and this might be attributed to the passivation of alloys [12, 28]. The mean values of cathodic Tafel slope (b_c) were much higher than the value of cathodic reaction controlled by oxygen reduction (about 120 mV·dec^{-1}) [36-39].

Table 2. Tafel extrapolation results and E_{pit} of potentiodynamic polarization curves of 2A12 aluminum alloy abraded with abrasive paper of various grit numbers.

Grit number	b_a (mV·dec^{-1})	b_c (mV·dec^{-1})	I_{corr} (μA·cm^2)	E_{corr} (mV)	E_{pit}(mV)
600	143±12.7	241±11.4	2.14±0.20	-910±18.0	-283±37.2
2000	156±15.3	269±4.2	1.11±0.63	-896±8.7	-212±14.0
5000	161±6.2	270±2.4	0.86±0.04	-824±18.3	-83±8.1

Since the test solution was aerated, the main cathodic reaction was still oxygen reduction. The potentiodynamic polarization tests pronounced that the smoother surface had lower corrosion susceptibility and better passivation performance compared to the rougher surface.

3.4 EIS measurements

The Nyquist and Bode plots of sanded samples after 3 h immersion in borate-buffered 0.0001 M NaCl solution are presented in Fig. 6.

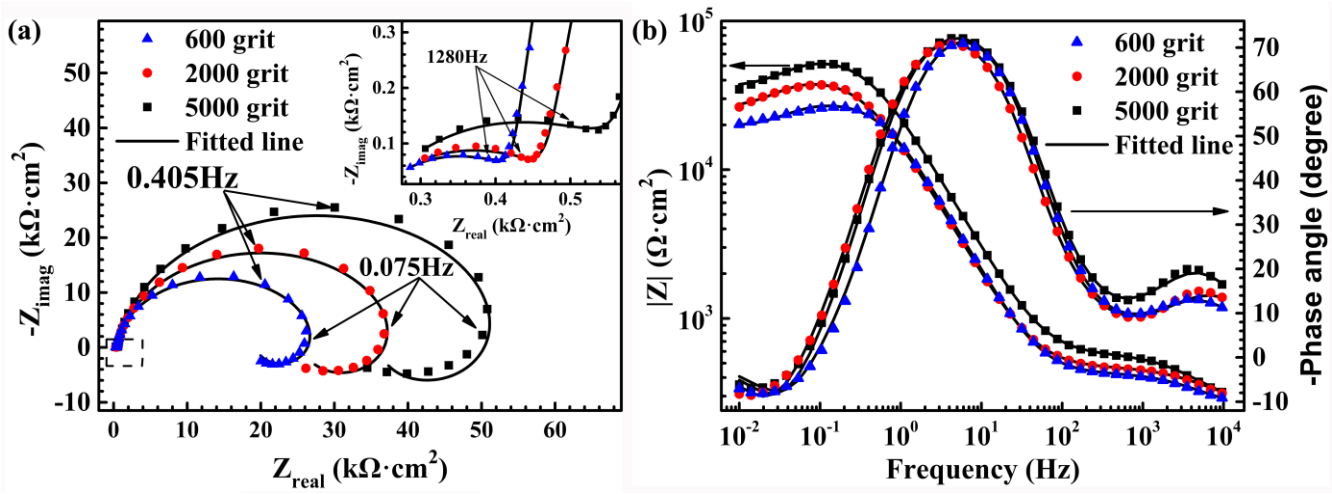

Figure 6. Nyquist plots (a) and corresponding Bode plots (b) of 2A12 aluminum alloy abraded with abrasive paper of various grit numbers.

The Nyquist plot showed similar depressed features. At high frequency range, all the EIS spectra exhibited a capacitive arc, indicating the presence of the passive film. Moreover, the capacitive arcs at intermediate frequencies were probably associated with pitting corrosion processes (metastable and stable). In addition, all the EIS spectra presented an inductive arc at low frequency range. In fact,

the origin of inductive features of electrochemical impedance was rather complicated. Generally, the presence of inductive features was associated with the surface relaxation process or absorption of intermediate corrosion product [2, 38, 40, 41]. In metal corrosion, the inductive features were often related to the weakening process of oxide film and corrosion induced by anodic dissolution of metals. Thus, the presence of inductive features manifested that all of the sanded samples underwent pitting corrosion after 3 h immersion. With increasing grit number from 600 to 5000, the increased radius of Nyquist loop revealed that the smoother surface had a better pitting corrosion resistance.

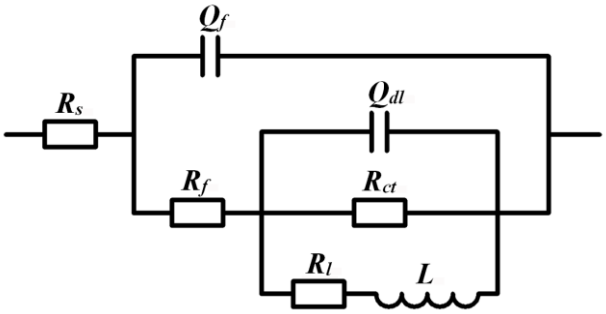

Figure 7. Equivalent circuit used to fit the EIS tests data, R_s is solution resistance, Q_f represents the CPE associated with the origin surface capacitance, R_f is the resistance of passive film, Q_{dl} represents the CPE associated with interfacial capacitance, R_{ct} is the charge transfer resistance, R_l and L are pseudo resistance and inductance.

In order to quantitatively estimate the pitting corrosion of 2A12 aluminum alloy abraded with abrasive paper of different grit numbers, the equivalent electrical circuit was adopted to fit the EIS spectra. The equivalent electrical circuit used in this study is presented in Fig. 7. In this equivalent electrical circuit, R_s is the electrolyte solution resistance; Q_f represents the constant phase element (CPE) associated with the origin surface capacitance at high frequency range; R_f is the resistance of passive film and corrosion products covered upon the pitting site; Q_{dl} represents the CPE associated with interfacial capacitance of the new interface originated from pitting at low frequency range; R_{ct} is the charge transfer resistance at active corroded surface, which is parallel to the Q_{dl} in low frequency range; R_l and L are pseudo resistance and inductance associated with breakdown of the passive film attacked by corrosive ions at low frequency range.

Table 3. Fitted value of in equivalent circuit of 2A12 aluminum alloy abraded with abrasive paper of various grit numbers.

Grit number	R_{hf} ($\Omega \cdot cm^2$)	R_{ct} ($k\Omega \cdot cm^2$)
600	188.3±9.9	27.6±1.29
2000	247.1±19.6	40.9±1.31
5000	343.8±27.8	47.5±6.84

Table 3 presents the fitted values of R_f and R_{ct} in equivalent electrical circuit. Both the values of R_f and R_{ct} increased with the increase of grit number. Firstly, the value of R_f was much smaller than that of passive film on aluminum alloys [8, 42]. As the parallel resistance of passive film and corrosion products on pit site, the value of R_f was determined by the smaller one. In this study, the value of R_f was determined by the resistance on pit site. Thus, as evidenced by the increased R_f, the air-formed passive film on the smoother surface had a better corrosion resistance than that formed on the rougher surface, which might be attributed to the less pits number and the smaller corroded area on the smoother surface. Moreover, since the increased R_{ct} indicated a higher resistance to active dissolution. The EIS tests demonstrated that the smoother surface showed lower pitting susceptibility and slower pitting propagation rate.

3.5 Metastable pits

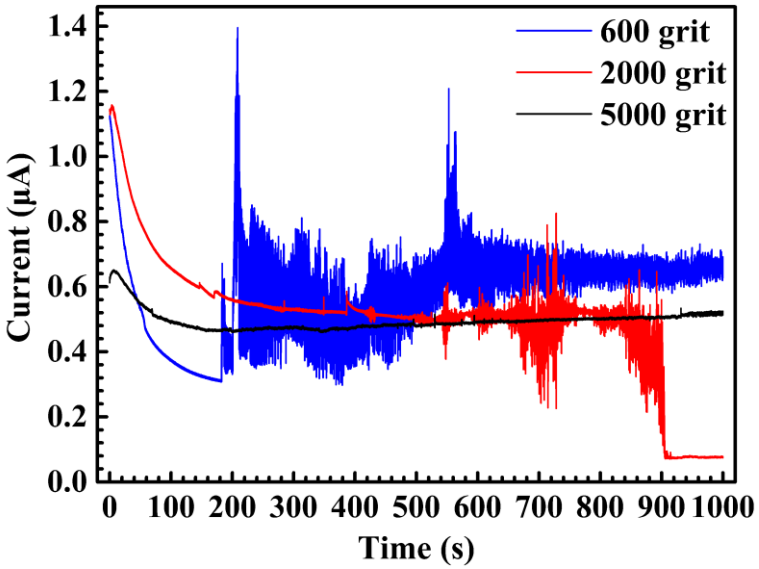

Figure 8. Current signatures obtained during potentiostatic polarization of 2A12 aluminum alloy abraded with abrasive paper of various grit numbers.

In order to estimate the metastable pitting, the potentiostatic polarization was performed on 1 mm diameter electrode at 100mV below the E_{pit} for 2A12 aluminum alloy abraded with abrasive papers of 600 grit, 2000 grit and 5000 grit. Featured current signatures obtained during potentiostatic polarization are presented in Fig. 8. Current transients could be detected superimposed on the background passive currents for all of the three kinds of electrodes. The current transients were mainly caused by initiation, propagation and repassivation of metastable pits. The current transient with anodic peaks and those with cathodic peaks were termed as anodic current transients and cathodic current transients. For the cathodic current transients, Burstein [43] revealed that their appearance could be attributed to the accelerated hydrogen evolution from Fe rich pit nucleation site. In this study, the cathodic current transients should be associated with the electron consuming reactions took place on S-phase [11, 29].

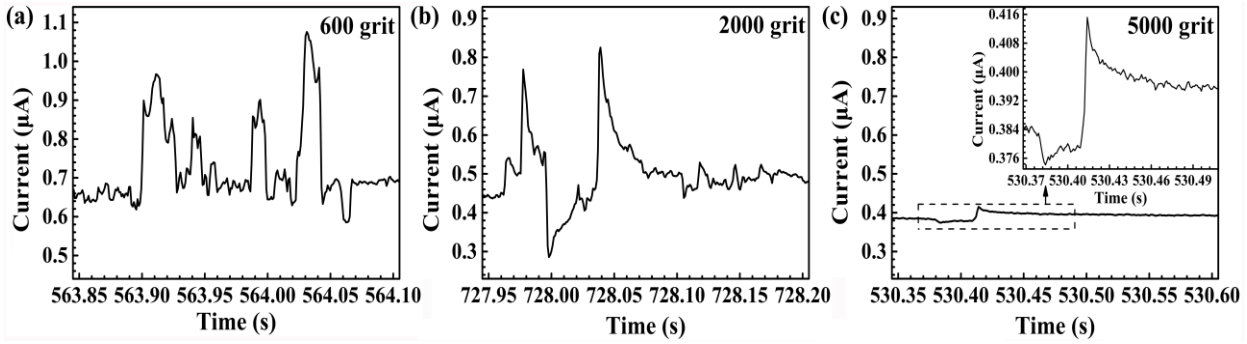

Figure 9. Anodic current transients obtained during potentiostatic polarization of 2A12 aluminum alloy abraded with abrasive papers of (a) 600 grit, (b) 2000 grit and (c) 5000 grit.

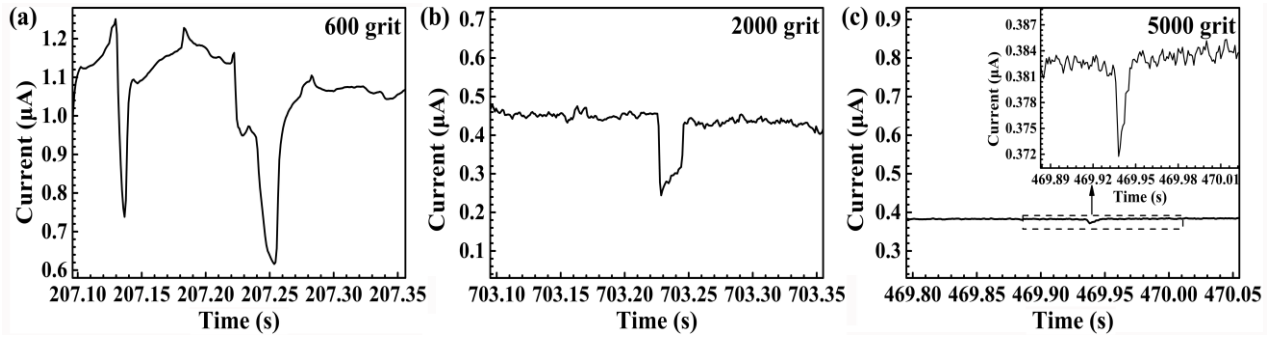

Figure 10. Cathodic current transients obtained during potentiostatic polarization of 2A12 aluminum alloy abraded with abrasive papers of (a) 600 grit, (b) 2000 grit and (c) 5000 grit.

Table 4. Statistical data of current transients in 2A12 aluminum alloy abraded with abrasive paper of different grit numbers.

Grit number	C_a	C_c	ΔI_a (nA)	ΔI_c (nA)	Δt_a (ms)	Δt_c (ms)
600	142±24.2	111±32.4	32.2±20.7	35.5±22.0	43.5±36.5	39.8±22.9
2000	51±17.9	22±11.6	30.0±23.1	35.0±15.0	29.1±23.1	28.9±11.1
5000	10±2.1	7±2.8	25.7±11.6	8.1±2.3	25.7±8.2	28.2±8.3

*C_a and C_c are the counts of anodic and cathodic current transients, respectively; ΔI_a and ΔI_c are the average peak value of anodic and cathodic current transients, respectively; Δt_a and Δt_c are average lifetime of anodic and cathodic current transients, respectively.

Detail views of the representative anodic and cathodic current transients are illustrated in Fig. 9 and 10, respectively. Both single peak and multiple peaks could be detected in anodic current transients, some of which exhibited a rapid rise in current and a relatively slow decay process, while others showed a sudden decay. These features were similar to those reported on aluminium alloy [11, 12, 43-45]. The sudden rise in current should be associated with the breakdown of passive film, and the followed current decay was associated with repassivation. For the multiple current peaks, they were probably caused by the initiation of several metastable pits at the same time or the changes of anolyte chemistry in one pit [45-47]. Similar to anodic current transients, the cathodic current

transients showed a sudden decay in current and followed by a rapid rise or slow rise. Obvious single peak could be found in some cathodic current transients, while others presented multiple cathodic peaks, which may be attributed to several cathodic reactions happening at the same time [12, 45]. Moreover, mixed current transients could also be found, seen in Fig. 9b and c. Their appearances were associated with the competition of the electron generation (metal dissolution) and consumption (hydrogen evolution or oxygen reduction) in the nucleated site [11].

Statistical data of the current transients are listed in Table 4. The frequency of anodic and cathodic current transients increased remarkably with the decrease of grit number, indicating that metastable pitting events occurred more frequently on the rougher surface. Furthermore, as the grit number increasing, the average peak value and average lifetime of anodic and cathodic current transients decreased significantly. This implied that the intensity of metastable pitting events increased as the grit number increasing from 600 to 5000. Compared to the smoother surface, though polarized at lower potential, the rougher surface exhibited more and larger current transients (anodic and cathodic), indicating metastable pitting events occurred more frequently and with greater intensity on the rougher surface. Current transient measurements revealed that metastable pits could initiate more easily and with bigger size on rougher surface.

3.6 Stable pits

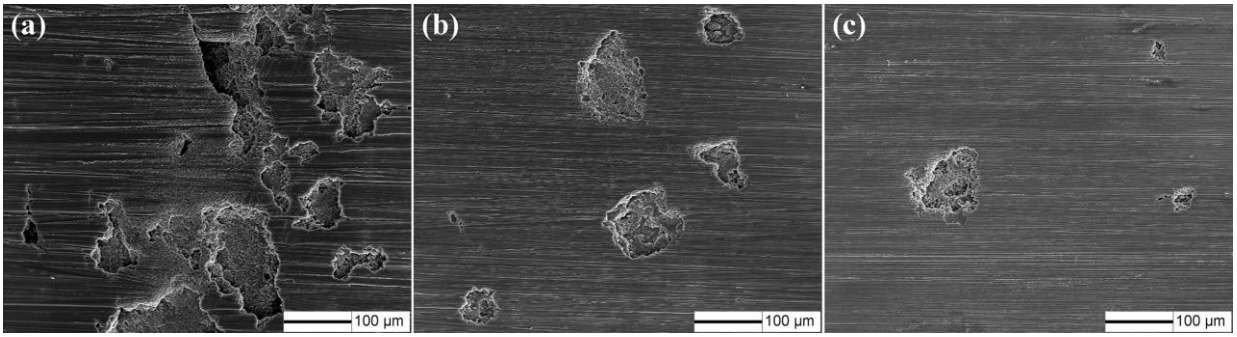

Figure 11. Morphologies of stable pits generated on 2A12 aluminum alloy abraded with abrasive papers of (a) 600 girt, (b) 2000 girt and (c) 5000 girt.

In order to evaluate the stable pitting of 2A12 aluminum alloy abraded to different grit numbers, the electrodes with surface area of 1cm^2 were potentiostatic polarized at E_{pit} with 3600s duration. Prior to corrosion area measurement, the corroded samples were ultrasonically cleaned in a mixture of 50 mL phosphoric + 20 g chromium trioxide + 950 mL deionized water and in pure water. Fig. 11 presents the morphologies of the pits on 2A12 aluminum alloy abraded to 600 grit, 2000 grit and 5000 grit. All of the sanded samples underwent pitting corrosion. Due to the corrosion of intermetallic particles and/or surrounding matrix, more speckles occurred on the rougher surface. Besides, surface layer dissolution (except pitting) was not observed for 2A12 aluminum alloy abraded with abrasive papers of 600 grit, 2000 grit and 5000 grit. Compared to the smoother surface, the rougher surface exhibited more and larger pits, indicating that pits could initiate more easily on the rougher surface.

For better evaluating the pitting on sanded samples, the pits mouth area was statistical analyzed. Fig. 12 shows the pits area distribution data (summation of 3 parallel electrodes). The number of pits on 2A12 aluminum alloy abraded to 600 grit, 2000 grit and 5000 grit were 991, 575 and 212, and average pits mouth area were 2052 μm^2, 1799 μm^2 and 1212 μm^2, respectively. The number of pits decreased with increasing grit number from 600 to 5000. Furthermore, the pits mouth area showed the same trend, i.e. decreased with the increase of grit number, implying that stable pits on the smoother surface had slower propagation rate than those on the rougher surface. Besides, according to Table 4, the current transients on the smoother surface had smaller peak value and shorter lifetime compared to those on the rougher surface.

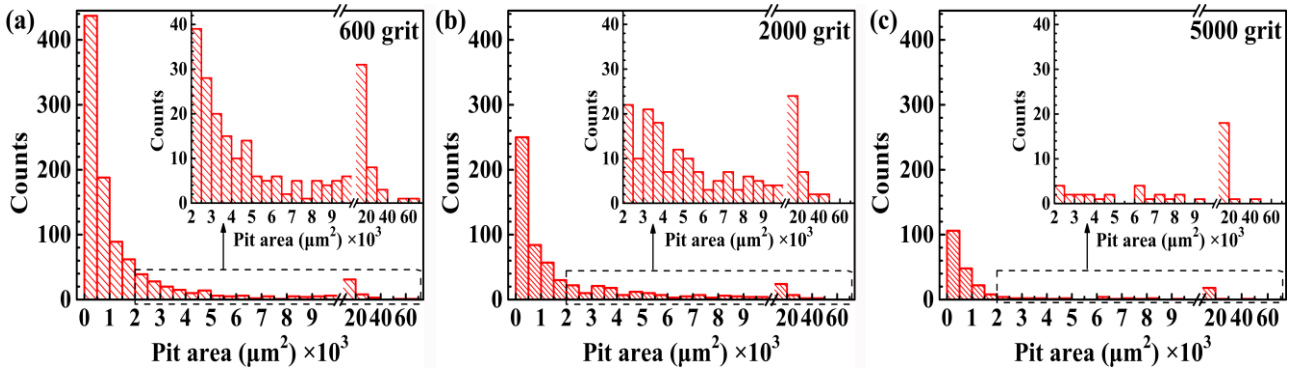

Figure 12. Size distribution histograms of stable pits on 2A12 aluminum alloy abraded with abrasive papers of (a) 600 girt, (b) 2000 girt and (c) 5000 girt.

Thus, the metastable pits on the rougher surface were larger in size and more likely to turn into stable pits, resulting in the formation of more and larger stable pits. Compared to the rougher surface, estimation of stable pits revealed that the smoother surface showed better pitting resistance because of its relatively lower pitting susceptibility and slower pit growth rate.

4. DISCUSSION

4.1 Effect of surface roughness on pitting

It is well known that surface abrasion can alter the surface roughness, which may have influence on pitting corrosion by altering the true surface area and the openness of surface grooves [48, 49]. Within the passive range, the critical passive current is expected to be proportional to the true surface area. However, the passive currents of samples abraded with abrasive papers of 600 grit, 2000 grit and 5000 grit are very similar in this study, revealing that the true surface area has relatively small effect on pitting corrosion of 2A12 aluminum alloy.

The openness of surface grooves is usually characterized by the aspect ratio of surface grooves ($w{\cdot}d^{-1}$), in which w and d are the width and depth of grooves at the opening, respectively. Statistical data of ten surface grooves on 2A12 aluminum alloy abraded by different grits abrasive papers are summarized in Table 5. With increase of surface roughness, both width and depth of the surface

grooves increase, while the aspect ratio of surface grooves decrease. The openness of surface grooves plays an important role on the diffusion of the dissolved corrosion products in the micro pits. The smaller value of $w \cdot d^{-1}$ implies that the groove is relatively narrow and deep, providing a deeper diffusion barrier. In narrow and deep grooves, corrosion products are more difficult to diffuse outward, resulting in a more severe acidification attributed to hydrolysis of metal ions [10, 12, 14]. Hence, the metastable pits emerged on the rougher surface could turn into stable pits more easily [10, 12, 14]. For metastable pits of stainless steel, the diffusion controlled model is well accepted. Therefore, the openness of surface grooves has significant influence on the pitting corrosion of stainless steel [44, 45, 48, 50]. Compared to those on the smoother surface, the metastable pits on the rougher surface have a better chance to obtain stable growth.

Table 5. The width, depth and aspect ratio of surface grooves for 2A12 aluminum alloy abraded with abrasive papers of different grit numbers.

Grit number	*w* (μm)	*d* (μm)	$w \cdot d^{-1}$
600	18.85±8.77	1.98±0.64	9.57±2.50
2000	11.85±5.07	0.78±0.14	15.18±5.83
5000	4.35±1.51	0.11±0.05	44.87±19.93

4.2 Effect of intermetallic particles on pitting

For Al and Al alloy, it is generally accepted that corrosion behavior is closely associated with intermetallic particles, grain size, residual stress, grain boundary precipitates and precipitate free zone [23, 29, 53, 54]. The major intermetallic particles in 2A12 aluminum alloy are S-phase, which are generally cathodic with respect to the matrix. In this study, the corrosion behavior of 2A12 aluminum alloy mainly relates to the density, area fraction and size of intermetallic particles.

As mentioned in Section 3.1, with increasing grit number from 600 to 5000, the density of S-phase decreases. As a cathodic particles, S-phase can drive dissolution of the surrounding matrix [30, 55]. Therefore, the frequencies of anodic and cathodic current transients decrease significantly with increasing grit number, i.e. the metastable pitting events occurred more frequently on the rougher surface. Moreover, metastable pitting (current transients) also closely relates to the size and area fraction of intermetallic particles. Compared to the smoother surface, both average size and area fraction of S-phase on the rougher surface are relatively larger, resulting in bigger current peak value and longer duration of anodic and cathodic current transients, because the dissolution of bigger particles or their surrounding matrix can induce bigger cavities. Besides, the precipitate size has effects on the stability of passive film, and then could affect the occurrence and formation of metastable pitting [56, 57]. Consequently, metastable pits initiate because the intermetallic particles above a critical size may lead to a defective passive film (oxide film). Compared to the smoother surface, the rougher surface promote the frequency of metastable pits and maintain the pits to propagate with a longer time, resulted from the bigger size, higher density and area fraction of particles on the rougher surface.

The metastable pit generated by the dissolution of big particles (and/or their surrounding matrix) could result in a deeper diffusion barrier and a more severe acidification [10, 12, 14, 58]. Thus, the metastable pits emerged around bigger particles could maintain continuous propagation more easily, indicating that the metastable pitting generated around bigger particles has a greater possibility turning into stable pitting. Besides, the frequency of metastable pitting (current transients) on rougher surface is higher than that on smoother surface. Therefore, both population and area of stable pits generated during 3600 s potentiostatic polarization increase with decreasing grit number of abrasive paper. The bigger size, higher density and area fraction of particles on the rougher surface promote the transition of pits from metastable to stable growth.

5. CONCLUSIONS

The microstructure and pitting corrosion of 2A12 aluminum alloy abraded with abrasive papers of 600 grit, 2000 grit and 5000 grit was studied. All of the sanded samples underwent pitting corrosion, while surface layer dissolution (except pitting) was not observed. The pitting corrosion of 2A12 aluminum alloy is strongly affected by the size, density and area fraction of intermetallic particles (S-phase). Whereas surface roughness shows relatively small influence on the pitting corrosion of 2A12 aluminum alloy.

(1) Surface abrasion can not only alter surface roughness, but also alter the size, density and area fraction of intermetallic particles. With increasing grit number from 600 to 5000, the surface roughness decreases, whilst the density, area friction and size of intermetallic particles in 2A12 aluminum alloy also decrease.

(2) One obvious breakdown potential, E_{pit}, exhibited in all the samples abraded with abrasive papers of 600 grit, 200 grit and 5000 grit. With increasing grit number from 600 to 5000, the decreased i_{corr}, the increased E_{pit}, R_f and R_{ct} indicates that 2A12 aluminum alloy exhibits lower corrosion susceptibility and better passivation performance.

(3) The frequency, peak value and lifetime of current transients decrease significantly with the decrease of grit number. With increasing grit number from 600 to 5000, the population and size of stable pits decrease remarkably. The enhanced density, higher area friction and bigger size of intermetallic particles on the rougher surface promote the initiation and growth of pits (metastable and stable). This indicates that with increasing grit number from 600 to 5000, 2A12 aluminum alloy exhibits lower corrosion susceptibility and lower pit growth rate.

References

1. M. Baig, H.R. Ammar, A.H. Seikh, M.A. Alam, and N.H. Alharthi, *Int. J. Electrochem. Sci.*, 12 (2017) 3336.
2. W. Tian, S. Li, J. Liu, M. Yu, and Y. Du, *Chinese J. Aeronaut.*, 30 (2017) 1777.
3. J. Kim, J. Jeun, H. Chun, Y.R. Lee, J. Yoo, J. Yoon, and H. Lee, *J. Alloy. Compd.*, 669 (2016) 187.

4. O.R. Perez, S. Valdez, A. Molina, S. Mejia-Sintillo, C. Garcia-Perez, V.M. Salinas-Bravo, and J.G. Gonzalez-Rodriguez, *Int. J. Electrochem. Sci.*, 12 (2017) 7300.
5. Y. Zhang, W. Fan, H.Q. Du, and Y.W. Zhao, *Int. J. Electrochem. Sci.*, 12 (2017) 6788.
6. Q.Q. Sun, J.G. Hu, J. Li, K.H. Chen, P.X. Dong, X.Z. Liao, and Y. Yang, *Int. J. Electrochem. Sci.*, 12 (2017) 5363.
7. S.W. Zou, Y.X. Zhang, W. Xu, Y.Q. Wan, C. He, C.F. Dong, and X.G. Li, *Int. J. Electrochem. Sci.*, 11 (2016) 9625.
8. J.A. Moreto, C.E.B. Marino, W.W. Bose Filho, L.A. Rocha, and J.C.S. Fernandes, *Corros. Sci.*, 84 (2014) 30.
9. M. Guerin, J. Alexis, E. Andrieu, L. Laffont, W. Lefebvre, G. Odemer, and C. Blanc, *Corros. Sci.*, 102 (2016) 291.
10. G.T. Burstein, C. Liu, R.M. Souto, and S.P. Vines, *Corros. Eng. Sci. Techn.*, 39 (2004) 25.
11. R.K. Gupta, N.L. Sukiman, M.K. Cavanaugh, B.R.W. Hinton, C.R. Hutchinson, and N. Birbilis, *Electrochim. Acta.*, 66 (2012) 245.
12. W. Tian, S. Li, B. Wang, J. Liu, and M. Yu, *Corros. Sci.*, 113 (2016) 1.
13. R.K. Gupta, B.R.W. Hinton, and N. Birbilis, *Corros. Sci.*, 82 (2014) 197.
14. G. Burstein, R. Souto, C. Liu, and S. Vines, *Mater. Corros.*, 29 (2004) S1.
15. K. Sasaki, and G.T. Burstein, *Corros. Sci.*, 49 (2007) 92.
16. S. Wang, J. Jiang, S. Dai, D.N. Seidman, G.S. Frankel, and L. Zhen, *J. Electrochem. Soc.*, 161 (2014) C433.
17. S. Wang, F. Yang, and G.S. Frankel, *J. Electrochem. Soc.*, 164 (2017) C317.
18. X. Zhou, Y. Liu, G.E. Thompson, G.M. Scamans, P. Skeldon, and J.A. Hunter, *Metall. Mater. Trans. A*, 42A (2011) 1373.
19. A. Afseth, J.H. Nordlien, G.M. Scamans, and K. Nisancioglu, *Corros. Sci.*, 43 (2001) 2359.
20. Y.W. Keuong, J.H. Nordlien, and K. Nisancioglu, *J. Electrochem. Soc.*, 148 (2001) B497.
21. R. Ambat, A.J. Davenport, A. Afseth, and G. Scamans, *J. Electrochem. Soc.*, 151 (2004) B53.
22. S. Wang, Y. Hu, K. Fang, W. Zhang, and X. Wang, *Corros. Sci.*, 126 (2017) 104.
23. P.J.E. Forsyth, *Mater. Sci. Tech.-Lond.*,14 (1998) 151.
24. X.J. Cai, W. Wei Ming, and M. Chen, *Advanced Materials Research*, 426 (2012) 321.
25. S. Wang, J. Jiang, G. Fan, L. Yang, S. Dai, G.S. Frankel, and L. Zhen, *Mater. Charact.*, 98 (2014) 18.
26. Z. Zhao, and G.S. Frankel, *Corros. Sci.*, 49 (2007) 3064.
27. S.P. Knight, N. Birbilis, B.C. Muddle, A.R. Trueman, and S.P. Lynch, *Corros. Sci.*, 52 (2010) 4073.
28. J. Lin, H. Liao, W. Jehng, C. Chang, and S. Lee, *Corros. Sci.*, 48 (2006) 3139.
29. R. Grilli, M.A. Baker, J.E. Castle, B. Dunn, and J.F. Watts, *Corros. Sci.*, 52 (2010) 2855.
30. A. Boag, R.J. Taylor, T.H. Muster, N. Goodman, D. Mcculloch, C. Ryan, B. Rout, D. Jamieson, and A.E. Hughes, *Corros. Sci.*, 52 (2010) 90.
31. A. Boag, A.E. Hughes, A.M. Glenn, T.H. Muster, and D. McCulloch, *Corros. Sci.*, 53 (2011) 17.
32. C.R. Hutchinson, P.T. Loo, T.J. Bastow, A.J. Hill, and J. Da Costa Teixeira, *Acta Mater.*, 57 (2009) 5645.
33. B.B. Straumal, B. Baretzky, A.A. Mazilkin, F. Phillipp, O.A. Kogtenkova, M.N. Volkov, and R.Z. Valiev, *Acta Mater.*, 52 (2004) 4469.
34. Y. Ustinovshikov, *J. Mater. Sci.*, 27 (1992) 3662.
35. S. Bai, Z. Liu, X. Zhou, Y. Gu, and D. Yu, *Scripta Mater.*, 64 (2011) 1133.
36. G.T. Burstein, and R.M. Organ, *Corros. Sci.*, 47 (2005) 2932.
37. G. T. Burstein, and C. Liu, *Corros. Sci.*, 37 (1995) 1151.
38. F. Song, X. Zhang, S. Liu, Q. Tan, and D. Li, *Corros. Sci.*, 78 (2014) 276.
39. S.L. Gojković, S.K. Zečević, M.D. Obradović, and D.M. DražIć, *Corros. Sci.*, 40 (1998) 849.
40. G.A. Zhang, L.Y. Xu, and Y.F. Cheng, *Electrochim. Acta.*, 53 (2008) 8245.

41. G.A. Zhang, L.Y. Xu, and Y.F. Cheng, *Corros. Sci.*, 51 (2009) 283.
42. F.J. Martin, G.T. Cheek, W.E. O Grady, and P.M. Natishan, *Corros. Sci.*, 47 (2005) 3187.
43. L. Speckert, and G.T. Burstein, *Corros. Sci.*, 53 (2011) 534.
44. L. Guan, Y. Zhou, H.Q. Lin, B. Zhang, J.Q. Wang, E.H. Han, and W. Ke, *Corros. Sci.*, 95 (2015) 6.
45. A.R. Trueman, *Corros. Sci.*, 47 (2005) 2240.
46. G.T. Burstein, and S.P. Mattin, *Phil. Mag. Lett.*, 66 (1992) 127.
47. P.C. Pistorius, and G.T. Burstein, *Corros. Sci.*, 36 (1994) 525.
48. Y. Zuo, H.T. Wang, and J.P. Xiong, *Corros. Sci.*, 44 (2002) 25.
49. G. T. Burstein, and P. Pistorius, *Corrosion*, 51 (1995) 380.
50. S.M. Lee, W.G. Lee, Y.H. Kim, and H. Jang, *Corros. Sci.*, 63 (2012) 404.
51. Y. Deng, R. Ye, G. Xu, J. Yang, Q. Pan, B. Peng, X. Cao, Y. Duan, Y. Wang, L. Lu, and Z. Yin, *Corros. Sci.*, 90 (2015) 359.
52. W. Tian, S. Li, X. Chen, J. Liu, and M. Yu, *Corros. Sci.*, 107 (2016) 211.
53. P. Leblanc, and G.S. Frankel, *J. Electrochem. Soc.*, 149 (2002) B239.
54. K.D. Ralston, N. Birbilis, M. Weyland, and C.R. Hutchinson, *Acta Mater.*, 58 (2010) 5941.
55. K.D. Ralston, N. Birbilis, M.K. Cavanaugh, M. Weyland, B.C. Muddle, and R.K.W. Marceau, *Electrochim. Acta.*, 55 (2010) 7834.
56. P.C. Pistorius, and G.T. Burstein, *Corros. Sci.*, 33 (1992) 1885.